

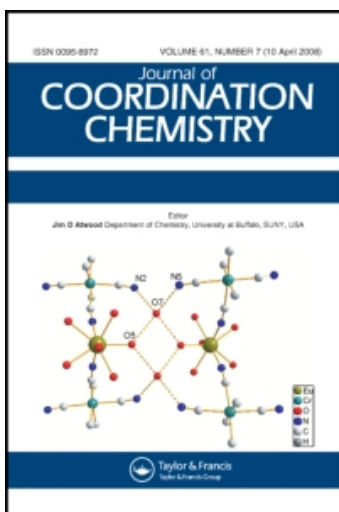
This article was downloaded by:

On: 22 January 2011

Access details: *Access Details: Free Access*

Publisher *Taylor & Francis*

Informa Ltd Registered in England and Wales Registered Number: 1072954 Registered office: Mortimer House, 37-41 Mortimer Street, London W1T 3JH, UK



Journal of Coordination Chemistry

Publication details, including instructions for authors and subscription information:

<http://www.informaworld.com/smpp/title~content=t713455674>

Structural characterization of the $\{3[\text{HBPMTU}]^+ \cdot 3[\text{X}]^- \cdot n\text{H}_2\text{O}\}$ salts (BPMTU = 1,3-bis(3-pyridylmethyl)-2-thiourea and X = Cl, Br, I). A polychlorine network based on $\text{O} \cdots \text{Cl}^-$ and $\text{OH} \cdots \text{Cl}^-$ interactions

I. I. Ozturk^a; S. K. Hadjikakou^a; A. C. Tsipis^a; G. Malandrinou^a; N. Kourkouvelis^b; M. J. Manos^c; A. J. Tasiopoulos^c; M. E. Light^d; M. Hursthouse^d; P. E. Bocanegra^e; I. S. Butler^e; N. Hadjiliadis^a

^a Department of Chemistry, Section of Inorganic and Analytical Chemistry, University of Ioannina, Ioannina 45110, Greece ^b Medical Physics Laboratory, Medical School, University of Ioannina, Ioannina 45110, Greece ^c Department of Chemistry, University of Cyprus, Nicosia 1678, Cyprus ^d Department of Chemistry, University of Southampton, Highfield, Southampton SO17 1BJ, UK ^e Department of Chemistry, McGill University, Montreal, Quebec H2A 2K6, Canada

First published on: 10 January 2011

To cite this Article Ozturk, I. I. , Hadjikakou, S. K. , Tsipis, A. C. , Malandrinou, G. , Kourkouvelis, N. , Manos, M. J. , Tasiopoulos, A. J. , Light, M. E. , Hursthouse, M. , Bocanegra, P. E. , Butler, I. S. and Hadjiliadis, N. (2011) 'Structural characterization of the $\{3[\text{HBPMTU}]^+ \cdot 3[\text{X}]^- \cdot n\text{H}_2\text{O}\}$ salts (BPMTU = 1,3-bis(3-pyridylmethyl)-2-thiourea and X = Cl, Br, I). A polychlorine network based on $\text{O} \cdots \text{Cl}^-$ and $\text{OH} \cdots \text{Cl}^-$ interactions', *Journal of Coordination Chemistry*, 64: 2, 202 – 221, First published on: 10 January 2011 (iFirst)

To link to this Article: DOI: 10.1080/00958972.2010.545123

URL: <http://dx.doi.org/10.1080/00958972.2010.545123>

PLEASE SCROLL DOWN FOR ARTICLE

Full terms and conditions of use: <http://www.informaworld.com/terms-and-conditions-of-access.pdf>

This article may be used for research, teaching and private study purposes. Any substantial or systematic reproduction, re-distribution, re-selling, loan or sub-licensing, systematic supply or distribution in any form to anyone is expressly forbidden.

The publisher does not give any warranty express or implied or make any representation that the contents will be complete or accurate or up to date. The accuracy of any instructions, formulae and drug doses should be independently verified with primary sources. The publisher shall not be liable for any loss, actions, claims, proceedings, demand or costs or damages whatsoever or howsoever caused arising directly or indirectly in connection with or arising out of the use of this material.

**Structural characterization of the
{3[HBPMU]⁺ · 3[X]⁻ · nH₂O} salts (BPMTU =
1,3-bis(3-pyridylmethyl)-2-thiourea and X = Cl, Br, I).
A polychlorine network based on O ... Cl⁻
and OH ... Cl⁻ interactions**

I.I. OZTURK[†], S.K. HADJIKAKOU*[†], A.C. TSIPIS[†], G. MALANDRINOS[†],
N. KOURKOUHELIS[‡], M.J. MANOS[§], A.J. TASIOPOULOS[§], M.E. LIGHT[¶],
M. HURSTHOUSE[¶], P.E. BOCANEGRA[⊥], I.S. BUTLER[⊥] and
N. HADJILIADIS*[†]

[†]Department of Chemistry, Section of Inorganic and Analytical Chemistry, University
of Ioannina, Ioannina 45110, Greece

[‡]Medical Physics Laboratory, Medical School, University of Ioannina,
Ioannina 45110, Greece

[§]Department of Chemistry, University of Cyprus, Nicosia 1678, Cyprus

[¶]Department of Chemistry, University of Southampton, Highfield,
Southampton SO17 1BJ, UK

[⊥]Department of Chemistry, McGill University, 801 Sherbrooke St. West,
Montreal, Quebec H2A 2K6, Canada

(Received 14 August 2010; in final form 27 October 2010)

Ionic salts with the formulae {3[HBPMU]⁺ · 3[X]⁻ · nH₂O} (BPMTU = 1,3-bis(3-pyridylmethyl)-2-thiourea, X = Cl⁻ and n = 1.5 (**1**), X = Br⁻ and n = 1 (**2**), X = I⁻ and n = 1 (**3**)) were synthesized. The compounds have been characterized by elemental analyses, TG-DTA, FT-IR, far-IR, Raman, ESI-MS and ¹H, ¹³C-NMR spectroscopic methods, and X-ray powder diffraction techniques. The crystal structures of **1** and **2** have also been determined by X-ray diffraction at 120(2) and 100(2) K, respectively. In **1**, weak lp(Cl⁻) → σ*(O-H) hyperconjugative interactions and OH ... Cl⁻ hydrogen-bonding interactions lead to the formation of 1-D zigzag tetrameric complexes consisting of four chlorides bridged by four waters. Two oxygens of the bridging waters are also coordinated to Cl⁻ of the complex forming a parallelogram-shaped ring. Two chlorides are also anchored by NH ... Cl⁻ hydrogen bonds in the free space between four tetrameric complexes. Heating **1** at 100°C for 4 h does not remove lattice water and the framework structure is retained. In **2**, NH ... Br⁻ hydrogen-bonding interactions stabilize the supramolecular architecture. In this case, however, only two bromides are bridged by one water through OH ... Br⁻ hydrogen bonds. The supramolecular interactions existing in the crystal packing of the ionic salts have been analyzed at the density functional theories and *ab initio* CCSD(T) levels of the theory.

Keywords: Inorganic chemistry; S Ligands – thioamides; Crystal structures; Computational study; DFT

*Corresponding authors. Email: shadjika@uoi.gr; nhadjis@uoi.gr

1. Introduction

Polymeric metallic or nonmetallic frameworks have emerged as a promising new class of materials, often containing crystalline, well-defined cavities or channels that can be used for the inclusion and exchange of various guest species [1]. Recently, a metal organic polymeric material containing channels functionalized with free carboxylic binding sites was found to act as a selective host for a $\text{Cl}(\text{H}_2\text{O})_4^-$ cluster [1a]. Urea-functionalized hydrogen-bonded helical frameworks have been studied as a new approach for separating anions from aqueous mixtures [1c]. Recently, we reported the synthesis and anti-proliferative activity of a series of organotin(IV) and antimony(III) complexes with thione/thiol [2–5a] or nucleotide [5b,c] ligands. In the course of our studies, the halogen salts of 1,3-bis(3-pyridylmethyl)-2-thiourea (BPMTU) with Cl^- , Br^- , I^- were accidentally isolated from the filtrate of the reaction with SbX_3 ($\text{X} = \text{Cl}, \text{Br}, \text{I}$) $\text{CH}_3\text{CN}/\text{CH}_3\text{OH}$ solutions showing interesting supramolecular architectures.

It should be noted here that the hydrochloride salt of a thiourea derivative, trovirdine (or pyridylethyl-4-bromopyridylthiourea) (LY300046) has been used as a non-nucleoside inhibitor of HIV-1 reverse transcriptase (RT) [2b,c]. In view of the possible biological importance of these salts, analogues of trovirdine, we decided to further characterize them and the present article reports on the structural, spectroscopic, and theoretical characterization of the ionic salts $\{3[\text{HBPMTU}]^+ \cdot 3[\text{X}]^- \cdot n\text{H}_2\text{O}\}$ ($\text{X} = \text{Cl}^-$ and $n = 1.5$ (**1**), $\text{X} = \text{Br}^-$ and $n = 1$ (**2**), $\text{X} = \text{I}^-$ and $n = 1$ (**3**)), accidentally isolated. An attempt to compare the liganding properties of 2-mercapto-benzimidazole (MBZIM) and HBPMTU toward SbCl_3 based on experimental and theoretical studies was made.

2. Results and discussion

2.1. General aspects

Besides complexes of formulae SbX_3L_2 or $\{[\text{SbX}_2\text{L}_4]^+\text{X}^-\}$ ($\text{X} = \text{Cl}^-$, Br^- , or I^- and $\text{L} = 2\text{-mercapto-benzimidazole (MBZIM), 5-ethoxy-2-mercapto-benzimidazole (EMBZIM), 2-mercapto-thiazoline (MTZD), or 2-mercapto-3,4,5,6-tetrahydro-pyrimidine (THMPM)}$) isolated from dichloromethane/methanolic or dichloromethane/acetonitrile solutions [4], slow evaporation of a MeOH/MeCN (1 : 1) solution derived by mixing a methanolic solution of SbX_3 ($\text{X} = \text{Cl}, \text{Br}, \text{I}$) with acetonitrile solutions of BPMTU (1 : 2), resulted in the formation of **1–3**. Compounds **1–3** are air-stable microcrystalline and are soluble in water, methanol, ethanol, DMSO, and DMF.

2.2. Protonation constants and species distribution

To investigate the acid–base properties of BPMTU, we have determined its protonation constants by potentiometry and the results are given in table 1. The species distribution diagram is shown in figure 1. Three protonation steps could be observed for free BPMTU, corresponding to the successive deprotonation of three functional groups. The fully protonated form of BPMTU can be considered as an H_3L^{3+} acid, due to the protonation of the two pyridyl nitrogens and sulfur. The lowest $\text{pK}\alpha_1$ value (1.73 for BPMTU) corresponds to protonated sulfur. In addition, the $\text{pK}\alpha_2$ and $\text{pK}\alpha_3$ values of

Table 1. Overall protonation constants and pK_a values of BPMTU at 25°C ($I=0.1 \text{ mol L}^{-1} \text{ KNO}_3$).

	Species	Log β^*	pK_a	Assignment
BPMTU	LH_3^{3*}	11.38 (0.03)	1.73	$\text{C}=\text{SH}^+$
	LH_2^{2*}	9.65 (0.01)	4.30	NH^+ (pyrimidine)
	LH^*	5.35 (0.01)	5.35	NH^+ (pyrimidine)

*Standard deviations are given in parenthesis.

$[\text{A}]_{\text{TOT}} = 2.00 \text{ mM}$

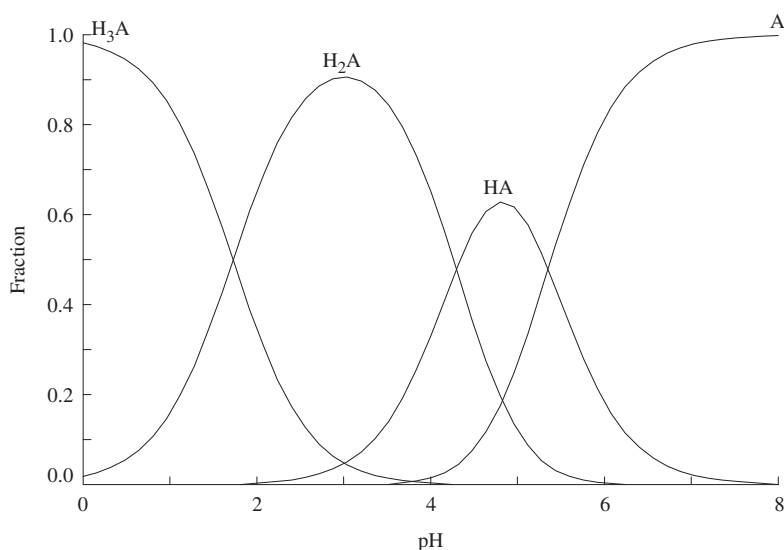


Figure 1. The species distribution diagram of BPMTU.

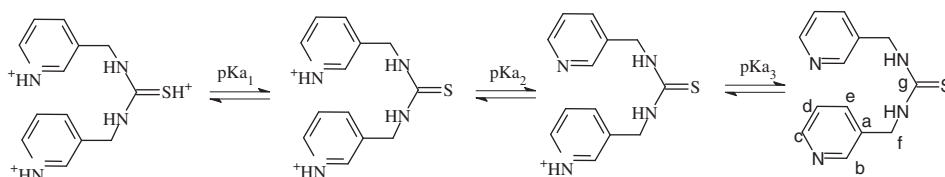
4.30 and 5.35 for BPMTU can be assigned to protonation of the two pyridyl groups (H_2L^{2+} and HL^+), in agreement with the corresponding values already published for pyridine (5.31 ± 0.01) [6a,b] (scheme 1).

The pK_a_3 value of 5.35 calculated for the deprotonation of nitrogen of BPMTU is higher than the pK_a value of 2.69 for the same type of ionization in 2-mercaptobenzimidazole (MBZIM) for which stable Sb-thione complexes, SbX_3L_2 or $\{\text{SbCl}_2\text{L}_4\}^+\text{X}^-$ ($\text{X} = \text{Cl}, \text{Br}$), were also recently reported [4a,b]. Therefore, the higher nitrogen proton affinity of BPMTU as compared to MBZIM resulted in easy formation of the corresponding salts besides stable complexes with SbX_3 [4].

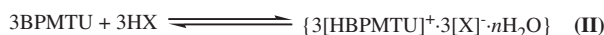
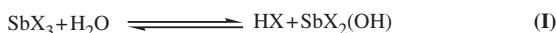
Based on these results and crystal structures (see also “X-ray crystallography” section 2.4) the following plausible mechanism for the formation of **1–3** could be proposed (scheme 2).

2.3. Structural and electronic properties of MBZIM and BPMTU

To understand the different ligating behaviors of the 2-mercaptobenzimidazole (MBZIM) and 1,3-bis(3-pyridylmethyl)-2-thiourea (BPMTU) toward the SbCl_3



Scheme 1. Ionization reactions of BPMTU.



BPMTU = 1,3-bis(3-pyridylmethyl)-2-thiourea,
 X = Cl⁻ and $n = 1.5$ (1), X = Br⁻ and $n = 1$ (2), X = I⁻ and $n = 1$ (3)

Scheme 2. Plausible mechanism for the formation of 1–3.

electrophile, we calculated the structural and selected electronic properties of the ligands using the full-range PBE0 non-local hybrid GGA functional [7–10] and the dispersion-corrected GGA B97-D functional developed by Grimme [11]. The performance of the B97-D functional for noncovalently bound systems including many pure van der Waals complexes is exceptionally good, reaching on the average CCSD(T) accuracy [11]. The equilibrium geometries of the MBZIM and BPMTU ligands computed at the PBE0/6-311++G(d,p) and B97D/6-311++G(d,p) levels of theory are shown in figure S1 given in ESI, while selected electronic parameters are compiled in table S1 given also in ESI.

The global minimum on the potential energy surface (PES) of MBZIM corresponds to the thione tautomeric form at both levels of theory, while the thiol form is a local minimum about 11 kcal mol⁻¹ higher in energy than the global minimum structure. Similar structures are predicted by the two levels of theory with the B97D functional giving structural parameters in closer resemblance with the experimental structure. The same holds true for the predicted structure of BPMTU (figure S1). The global minimum structure of BPMTU corresponds to the *syn*-conformer with the *anti*-one being a local minimum only about 1.0 kcal mol⁻¹ higher in energy illustrating free rotation around the thioamide C–N bond and coexistence of both conformers in solution. The C=S bond length in the thione tautomeric form of MBZIM was found to be 1.655 and 1.664 Å at the PBE0/6-311++G(d,p) and B97D/6-311++G(d,p) levels, respectively. Noteworthy is the excellent agreement of the C=S bond lengths of the *syn*-conformer of BPMTU ligand, predicted to be 1.678 and 1.689 Å at the PBE0/6-311++G(d,p) and B97D/6-311++G(d,p) levels, respectively, with the experimental value [12] of 1.6920(17) Å.

To assess the ligating ability of MBZIM and BPMTU we estimated the nucleophilicity ω^- of the ligands with respect to SbCl₃, given by [13]

$$\omega^- = \frac{1}{2} \frac{(\mu_A - \mu_B)^2}{(\eta_A + \eta_B)^2} \eta_A,$$

where μ_A and μ_B are the chemical potential μ of the nucleophile (A) and electrophile (B), respectively, $\mu = (\varepsilon_{\text{LUMO}} + \varepsilon_{\text{HOMO}})/2$ and η_A and η_B are the hardness η of the nucleophile (A) and electrophile (B), respectively, $\eta = \varepsilon_{\text{LUMO}} - \varepsilon_{\text{HOMO}}$.

The estimated nucleophilicity ω^- for the thione (thiol) tautomeric forms of MBZIM was found to be 0.096 (0.101) and 0.067 (0.070) eV at the B97D/6-311++G(d,p) and PBE0/6-311++G(d,p) levels, respectively. On the other hand, the estimated nucleophilicity for the *syn*- (*anti*-) conformers of BPMTU was 0.072 (0.073) and 0.049 (0.045) eV at the B97D/6-311++G(d,p) and PBE0/6-311++G(d,p) levels, respectively. MBZIM is a stronger nucleophile than BPMTU. Furthermore, the Mulliken net atomic charge on the sulfur donor of the thione (thiol) tautomeric forms of MBZIM was -0.74 (-0.56) and -0.79 (-0.59) |e| at the B97D/6-311++G(d,p) and PBE0/6-311++G(d,p) levels, respectively. Accordingly the Mulliken net atomic charge on the sulfur of the *syn*- (*anti*-) conformers of BPMTU was -0.01 (0.01) and -0.61 (-0.71) |e| at the B97D/6-311++G(d,p) and PBE0/6-311++G(d,p) levels, respectively. Interestingly, the sulfur donor of the *syn*- conformer (the experimentally isolated conformer) of BPMTU is practically neutral, while that of the thione tautomeric form of MBZIM acquires a negative charge around -0.75 |e|. Both the higher nucleophilicity and the high net negative atomic charge on sulfur of the MBZIM accounts well for its high ligating ability to form a variety of complexes reported previously. In contrast, the lower nucleophilicity of BPMTU in conjunction with the neutrality of the sulfur donor explains why this ligand is not coordinated to SbCl_3 , but affords water-soluble ionic salts.

2.4. Crystal and molecular structures of $\{3[\text{HBPMTU}]^+ \cdot 3[\text{Cl}]^- \cdot 1.5\text{H}_2\text{O}\}$ (1) and $\{3[\text{HBPMTU}]^+ \cdot 3[\text{Br}]^- \cdot \text{H}_2\text{O}\}$ (2)

ORTEP diagrams of **1** and **2** as well as selected bond distances and angles are shown in figures 2 and 3.

In the unit cell of **1** there are three cation–anion pairs and one water. The cation originated from the protonation of BPMTU at one of the two pyridyl nitrogens. The positively charged HBPMTU⁺ residue interacts with one Cl[−] counter anion. Strong NH...Cl[−] and OH...Cl[−] hydrogen-bonding interactions along with quite strong O...Cl[−] interactions stabilize the supramolecular architecture (figure 4a). The relative O...Cl[−] distance **R** calculated by the relationship $\mathbf{R} = d/(r_X + r_D)$ (d is the observed O...X[−] distance and r_X and r_D (or r_{ion}) are standard VDW radii of the involved atoms (or ions)) ($r_{\text{Cl}^-} = 1.81 \text{ \AA}$, $r_{\text{Br}^-} = 1.96 \text{ \AA}$, $r_{\text{O}} = 1.52 \text{ \AA}$) [14] suggested by Lommerse *et al.* [15] was found to be 0.86 illustrating quite strong O...Cl[−] interactions. The hydrogen bonds are as follows: N2...Cl1i = 3.203(2) Å, N3...Cl1ii = 3.218(2) Å, N10...Cl1iii = 3.280(2) Å, N11...Cl1iii = 3.351(2) Å, N7...Cl2 = 3.257(2) Å, O1...Cl2iv = 3.064(2) Å, and O1...Cl3 = 3.113(2) Å. (Symmetry transformations used to generate equivalent atoms: (i) $-x, -y, -z + 1$, (ii) $x, y, z - 1$, (iii) $x + 1/2, -y + 1/2, z - 1/2$, (iv) $x - 1/2, -y + 1/2, z - 1/2$) (figure 4). Particularly, the weak O...Cl[−] interactions (2.878 Å) and the strong OH...Cl[−] (2.258 Å) hydrogen-bonding interactions lead to the formation of 1-D zigzag tetrameric complexes consisting of four chlorides bridged by four waters through hydrogen bonds (figure 4b). Two oxygens of bridging waters are also coordinated to Cl[−] of the complex forming a rhombus-shaped ring. The 1-D tetrameric chains are terminated by two

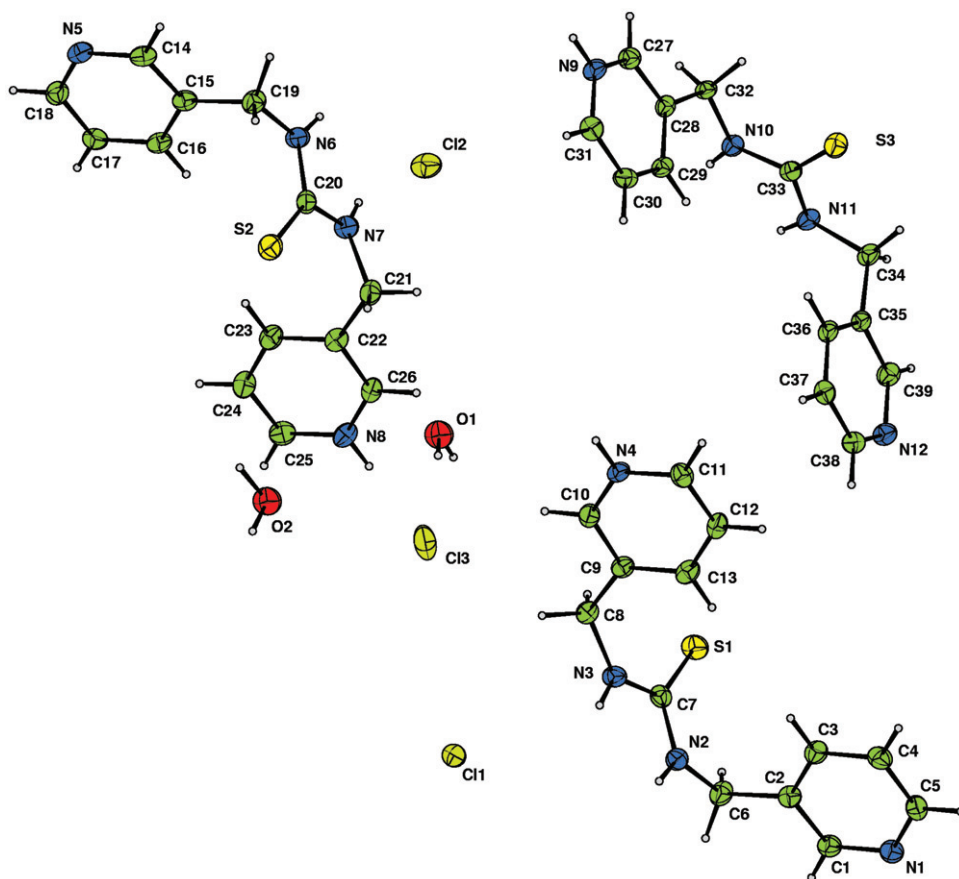


Figure 2. ORTEP diagram of **1** together with the atomic numbering scheme. Thermal ellipsoids drawn at the 50% probability level. Selected bond lengths (Å), angles (°) and torsion angles (°); First cation–anion pair; S1C7 = 1.683(3), N2–C7 = 1.348(3), N2–C6 = 1.446(3), N3–C7 = 1.354(3), N3–C8 = 1.450(3), N1–C1 = 1.343(3), N1–C5 = 1.345(3), N4–C10 = 1.333(3), N4–C11 = 1.346(3), N2–C7–S1 = 123.2(2), N3–C7–S1 = 123.0(2), N2–C7–N3 = 113.9(2). Second cation–anion pair; S2–C20 = 1.680(3), N6–C20 = 1.352(3), N6–C19 = 1.448(3), N7–C20 = 1.350(3), N7–C21 = 1.451(3), N5–C18 = 1.339(4), N5–C14 = 1.349(4), N8–C26 = 1.334(3), N8–C25 = 1.339(4), N7–C20–S2 = 122.6(2), N6–C20–S2 = 122.7(2), N7–C20–N6 = 114.7(2). Third cation–anion pair; S3–C33 = 1.688(3), N10–C33 = 1.352(3), N10–C32 = 1.449(3), N11–C33 = 1.351(3), N11–C34 = 1.456(3), N9–C27 = 1.334(3), N9–C31 = 1.345(3), N12–C38 = 1.338(4), N12–C39 = 1.346(3), N11–C33–N10 = 113.4(2), N11–C33–S3 = 124.0(2), N10–C33–S3 = 122.62(19).

NH...Cl⁻ hydrogen bonds from two HBPMTU⁺ ligands. Two chlorides are captured in the free space between four tetrameric complexes of the crystal lattice, forming {[Cl(OH₂)⁻]₄}₂Cl⁻ units (figure 4b) through hydrogen bonds. The Cl...Cl distance of these chlorides being 3.830 Å is slightly longer than the sum of van der Waals radii (3.62 Å) [14], thus reflecting the non-existence of closed-shell Cl⁻...Cl⁻ interactions. The highest occupied molecular orbital (HOMO) of the [HBPMTU]⁺ [Cl⁻...Cl⁻] fragment with Cl⁻ anions hanging on the NH hydrogens of [HBPMTU]⁺ being an antibonding σ* MO localized on the [Cl⁻...Cl⁻] moiety (scheme 3) further supports the non-existence of closed-shell Cl⁻...Cl⁻ interactions in **1**. One Cl⁻ is anchored by four NH...Cl⁻ hydrogen bonds creating a noncovalent distorted tetrahedral

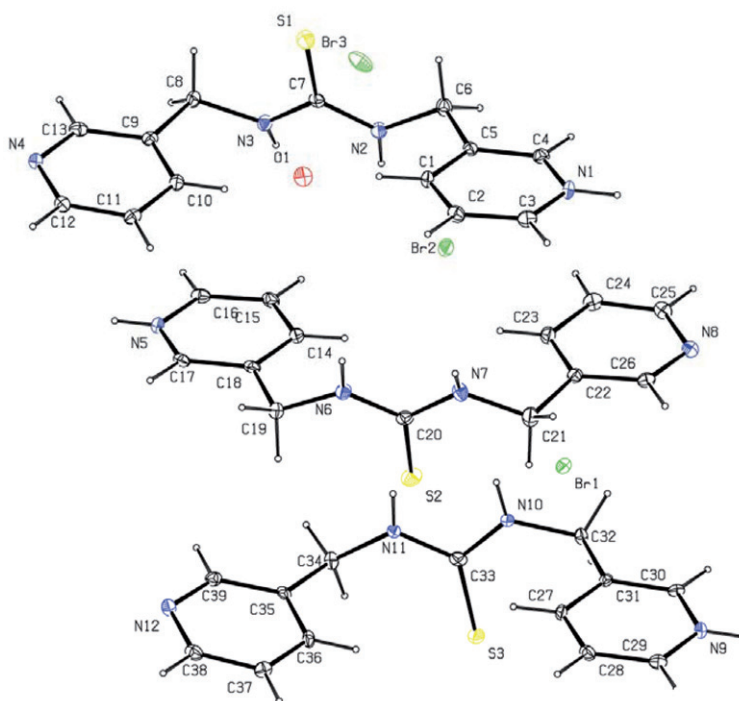
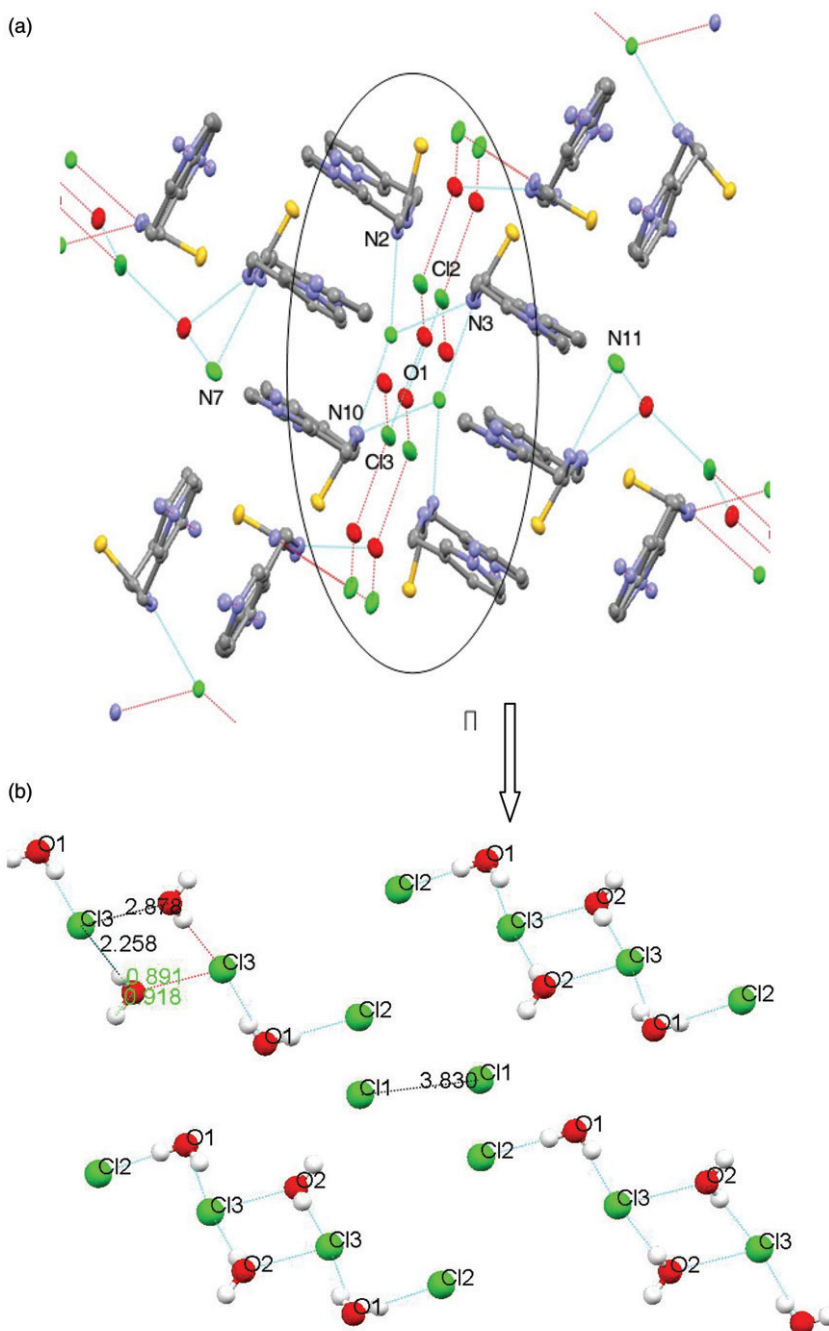
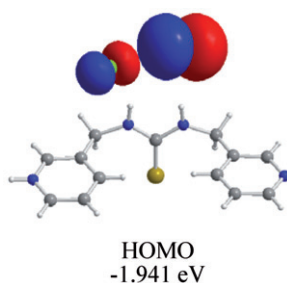
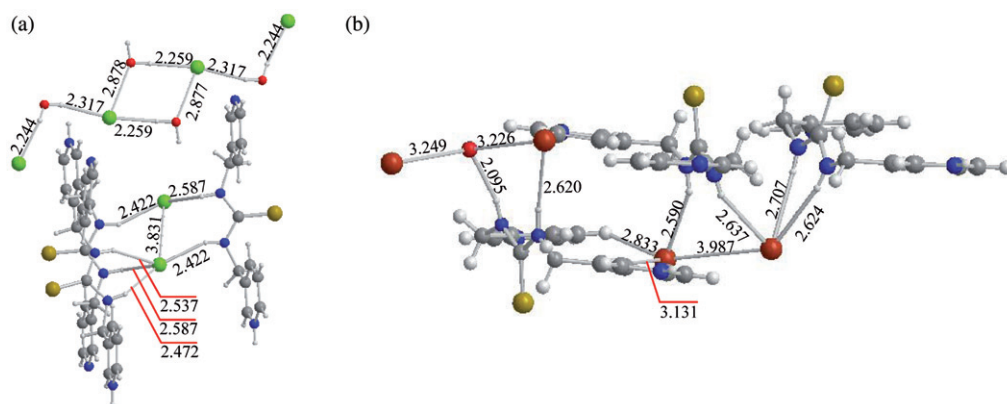


Figure 3. ORTEP diagram of **2** together with the atomic numbering scheme. Thermal ellipsoids drawn at the 50% probability level. Selected bond lengths (Å), angles ($^{\circ}$), and torsion angles ($^{\circ}$); First cation-anion pair; S1–C7 = 1.679(3), N1–C3 = 1.334(4), N1–C4 = 1.332(4), N4–C13 = 1.340(4), N4–C12 = 1.334(4), S1–C7–N3 = 123.1(3), S1–C7–N2 = 122.4(3), N2–C–N3 = 114.5(3). Second cation-anion pair; S2–C20 = 1.684(3), N5–C17 = 1.335(4), N5–C16 = 1.333(4), N8–C26 = 1.336(4), N8–C25 = 1.342(4), S2–C20–N6 = 122.9(3), S2–C20–N7 = 123.2(3), N6–C20–N7 = 114.0(3). Third cation-anion pair; S3–C33 = 1.689(3), N12–C39 = 1.340(4), N12–C38 = 1.340(4), N9–C29 = 1.338(4), N9–C30 = 1.334(4), S3–C33–N11 = 123.9(3), S3–C33–N10 = 122.4(3), N10–C33–N11 = 113.6(3).

coordination sphere around Cl^- , while the other Cl^- is anchored by two $\text{NH}\cdots\text{Cl}^-$ hydrogen bonds adopting a V-shaped coordination sphere ($\text{H}\cdots\text{Cl}^-\cdots\text{H}$ bond angle of 115.5°). The supramolecular interactions in the crystal lattices of the ionic salts **1** and **2** are depicted schematically in scheme 4.

The average C–S bond distance is *ca* 1.68 Å (S1C7 = 1.683(3), S2–C20 = 1.680(3), S3–C33 = 1.688(3) Å, respectively) indicating a thione form for **1**. The C–S bond distance in free BPMTU is 1.6920(17) [12], slightly longer than the corresponding one found in **1** (1.68 Å). The C–N bond lengths in pyridyl rings are almost identical (1.34 Å) in the case of the non-protonated rings (N1–C1 = 1.343(3), N1–C5 = 1.345(3), N5–C18 = 1.339(4), N5–C14 = 1.349(4), N12–C38 = 1.338(4), N12–C39 = 1.346(3) Å), while in the case of the protonated ring these C–N distances slightly varied between 1.33 and 1.34 Å (N4–C10 = 1.333(3), N4–C11 = 1.346(3), N8–C26 = 1.334(3), N8–C25 = 1.339(4), N9–C27 = 1.334(3), N9–C31 = 1.345(3) Å) due to protonation. The average C–N distance of the free ligand is 1.34 Å (N2–C6 = 1.337(3), N2–C7 = 1.337(3), N4–C13 = 1.341(3), N4–C12 = 1.331(3) Å) [12]. The N–C–S bond angle is close to 123° (N2–C7–S1 = 123.2(2), N3–C7–S1 = 123.0(2), N7–C20–S2 = 122.6(2), N6–C20–S2 = 122.7(2), N11–C33–S3 = 124.0(2), N10–C33–S3 = 122.62(19) $^{\circ}$, respectively). The N–C–N bond



Scheme 3. HOMO of the $[\text{HBPMTU}]^+ [\text{Cl}^- \cdots \text{Cl}^-]$ fragment.Scheme 4. Supramolecular interactions in the crystal lattice of the ionic salts **1** (a) and **2** (b).

angles are almost 114° ($\text{N}2\text{--C}7\text{--N}3 = 113.9(2)^\circ$, $\text{N}7\text{--C}20\text{--N}6 = 114.7(2)^\circ$, $\text{N}11\text{--C}33\text{--N}10 = 113.4(2)^\circ$). This discrepancy from the ideal 120° for sp^2 hybrid is due to lower electron pair repulsion between the electrons of the nitrogens of C–N bonds compared to those electrons of the corresponding carbon–sulfur bonds due to the higher electronegativity of the former. The corresponding bond angles for the free ligand are $\text{N--C--S} = 122^\circ$ and $\text{N--C--N} = 115.6^\circ$ [12].

In the unit cell of **2** there are also three cation–anion pairs and one water (figure 3). Similarly with **1**, the cation of **2** originates from protonation of BPMTU on one of the two pyridyl nitrogens. The positively charged HBPMTU^+ residue interacts with a Br^- .

The average C–S bond distance in **2** is *ca* 1.68 \AA ($\text{S}1\text{--C}7 = 1.679(3)$, $\text{S}2\text{--C}20 = 1.684(3)$, $\text{S}3\text{--C}33 = 1.689(3) \text{ \AA}$), which is close to the corresponding C–S bond distances found in the free ligand ($1.6920(17)$ [12]). The C–N bond lengths of the pyridyl rings are almost identical (1.34 \AA) for non-protonated rings ($\text{N}4\text{--C}13 = 1.340(4)$, $\text{N}4\text{--C}12 = 1.334(4)$, $\text{N}8\text{--C}26 = 1.336(4)$, $\text{N}8\text{--C}25 = 1.342(4)$, $\text{N}12\text{--C}39 = 1.340(4)$, $\text{N}12\text{--C}38 = 1.340(4) \text{ \AA}$). In the case of the protonated ones, the two C–N distances are also almost equal (average 1.33 \AA) ($\text{N}1\text{--C}3 = 1.334(4)$, $\text{N}1\text{--C}4 = 1.332(4)$, $\text{N}5\text{--C}17 = 1.335(4)$, $\text{N}5\text{--C}16 = 1.333(4)$, $\text{N}9\text{--C}29 = 1.338(4)$, $\text{N}9\text{--C}30 = 1.334(4) \text{ \AA}$, respectively) in contrast to the corresponding ones of **1**. The N–C–S bond angles are close to

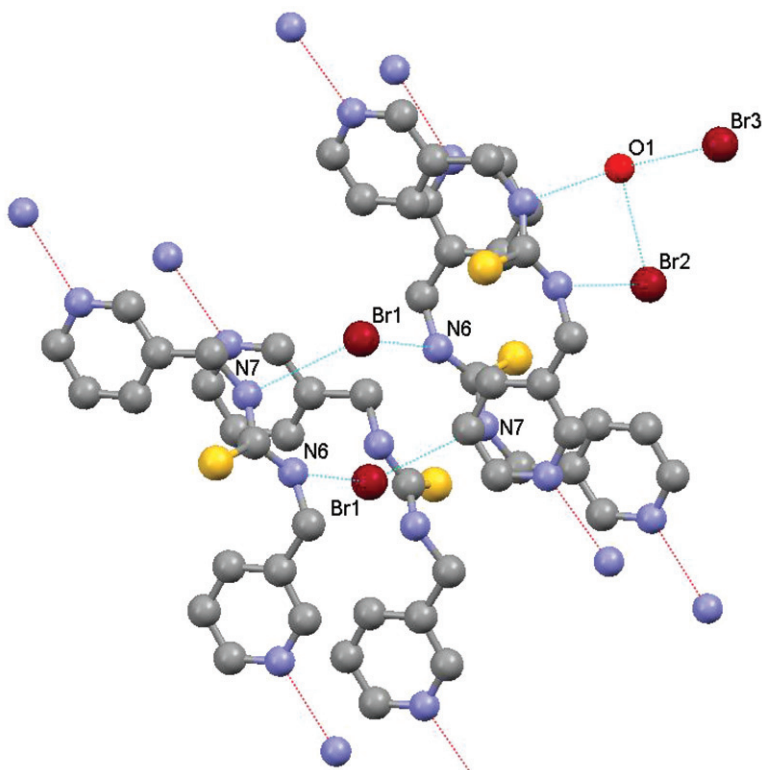


Figure 5. Packing diagram of **2** where weak hydrogen-bonding interactions are observed. Hydrogen bonds (Å): N2...Br2 = 3.392(3), N3...O1 = 2.916(3), N6...Br1 = 3.350(3), N7...Br1 = 3.331(3), Br3...O1 = 3.249(2).

123° (S1–C7–N3 = 123.1(3), S1–C7–N2 = 122.4(3), S2–C20–N6 = 122.9(3), S2–C20–N7 = 123.2(3), S3–C33–N11 = 123.9(3), S3–C33–N10 = 122.4(3)°). Hydrogen bonds are also observed in **2** (N2...Br2 = 3.392(3), N3...O1 = 2.916(3), N6...Br1 = 3.350(3), N7...Br1 = 3.331(3), Br3...O1 = 3.249(2), respectively) (figure 5, scheme 4b).

The Br[−]...Br[−] distance of 3.987 Å is slightly longer than the sum of van der Waals radii (3.92 Å) [14], thus reflecting the non-existence of closed-shell Br[−]...Br[−] interactions and prove that the $R=1.017$ in **2** does not represent Br[−]...Br[−] interactions. On the other hand, the O...Br[−] distance of 3.226 Å is slightly shorter than the sum of van der Waals radii (3.48 Å) [14], indicating weak O...Br[−] interaction (scheme 4b). The weaker O...Br[−] interactions compared to the O...Cl[−] is also reflected in relative O...Br[−] distance $R=0.93$ (compared to $R=0.86$ for O...Cl[−]).

2.5. Vibrational spectroscopy

In order to further investigate the ability of the amido hydrogens of HBPMTU⁺ to act as anchors for the two Cl[−] anions captured in the free space between four tetrameric complexes of the crystal lattice of **1**, Raman and far-infrared (IR) spectra of **1–3** were

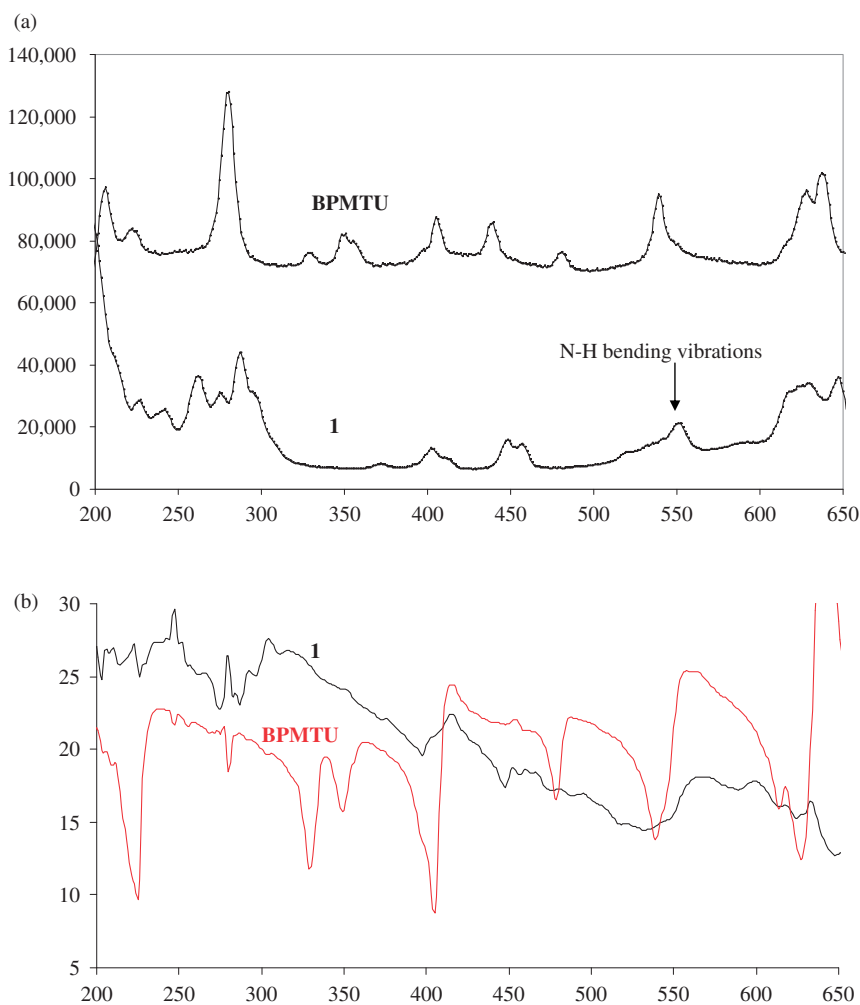
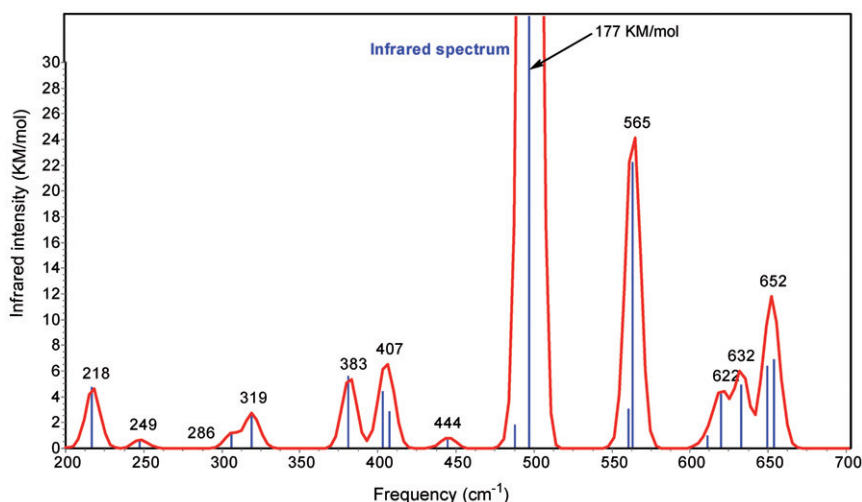


Figure 6. Raman (a) and far-IR (b) spectra of **1** and free BPMTU.

recorded (figure 6). The IR spectrum of “free” BPMTU computed at the B97D/6-311++G(d,p) and PBE0/6-311++G(d,p) levels of theory showed a relatively strong band with peak maximum at 503.0 and 497.5 cm^{-1} , respectively, due to N–H bending vibrations shown in scheme 5.

In accordance with other evidence, no band due to $\nu(\text{Cl}^- \cdots \text{Cl}^-)$ around 500 cm^{-1} was observed in the IR spectrum of **1**. The weak band at 550 cm^{-1} in the Raman spectrum of **1** is attributed to N–H bending vibrations of HBPMTU^+ . The stretching vibration of Cl_2 in the solid state [16a] absorbs at 540.0 cm^{-1} . The Raman spectrum of Cl_2 in the gas calculated at the PBE0/6-311++G(d,p) level showed the stretching vibration peak at 549.0 cm^{-1} . On the other hand, we calculated the Raman spectrum for the $\text{Cl}^- \cdots \text{Cl}^-$ moiety found in the crystal lattice of **1** and the $\nu(\text{Cl}^- \cdots \text{Cl}^-)$ stretching vibration was predicted to absorb at 71.7 cm^{-1} at the CCSD(T)/6-311+G(d) level of theory. High-pressure Raman spectra show a strengthening of the vibrational band at



Scheme 5. The 200–700 cm^{-1} part of the IR spectrum of “free” BPMTU showing the N–H bending vibrations around 500 cm^{-1} .

550 cm^{-1} , which is shifted by 7 cm^{-1} from 548 to 555 cm^{-1} with an increasing pressure (0–4 GPa) and an increase in intensity from 2281 to 3636 UA, suggesting an increase in $\text{NH}\cdots\text{Cl}^-$ interaction with increasing pressure (figure 7). Moreover, no Cl_2 evolution was observed under the pressure used. The band at 580 cm^{-1} in the far-IR spectrum of **1** is also assigned to the N–H bending vibrations of HBPMTU^+ (figure 6b). We also calculated the Raman spectrum of the $\text{Br}^- \cdots \text{Br}^-$ moiety found in the crystal lattice of **2** and the $\nu(\text{Br}^- \cdots \text{Br}^-)$ stretching vibration was predicted to absorb at 49.5 cm^{-1} at the CCSD(T)/6-311+G(d) level of theory. These low values calculated in both complexes for the $\nu(\text{X}^- \cdots \text{X}^-)$ indicate the non-existence of such interaction.

2.6. Thermal decomposition and X-ray powder diffraction study

For the XRPD and thermal analysis experiments powdered samples were used for **1–3**, obtained by grinding single crystals (in cases of **1** and **2**). TG/DTA analysis (under nitrogen) of **1** shows that the compound is stable to 200°C and then decomposes with an endothermic peak between 200°C and 500°C corresponding to the loss of two BPMTU ligands, two chlorines and all water (found: 68%, Calcd 68%) and an exothermic peak at higher than 500°C corresponding to one BPMTU and one chlorine (found: 30%, Calcd 32%). TG/DTA analyses of **2** and **3** show that these compounds are stable to 200°C and then decompose progressively in one endothermic step.

The XRPD patterns show that the structure of **1** (figure 8a) is essentially retained upon heating in agreement with TG analysis. In order to investigate this point further, a sample of **1** was heated at 100°C for 4 h and the XRPD pattern recorded was identical to that of the original sample (figure 8b). Thus, the water molecules cannot be removed from the lattice since **1** retains its structure. This is probably due to the strong hydrogen-bonding interactions involving water,

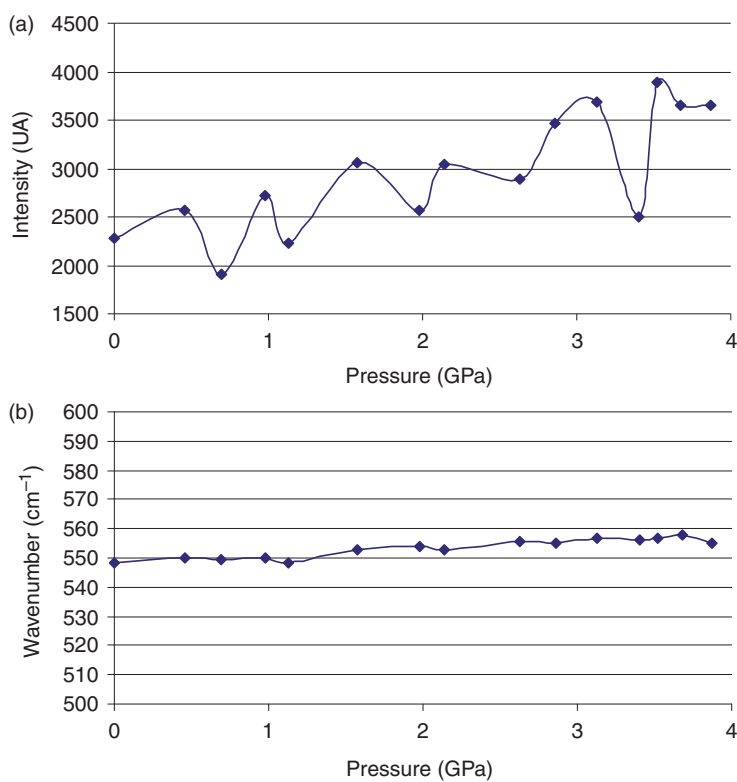


Figure 7. (a) Intensity of the band at 550cm^{-1} vs. pressure in case of **1**. (b) wavenumber vs. pressure in case of **1**.

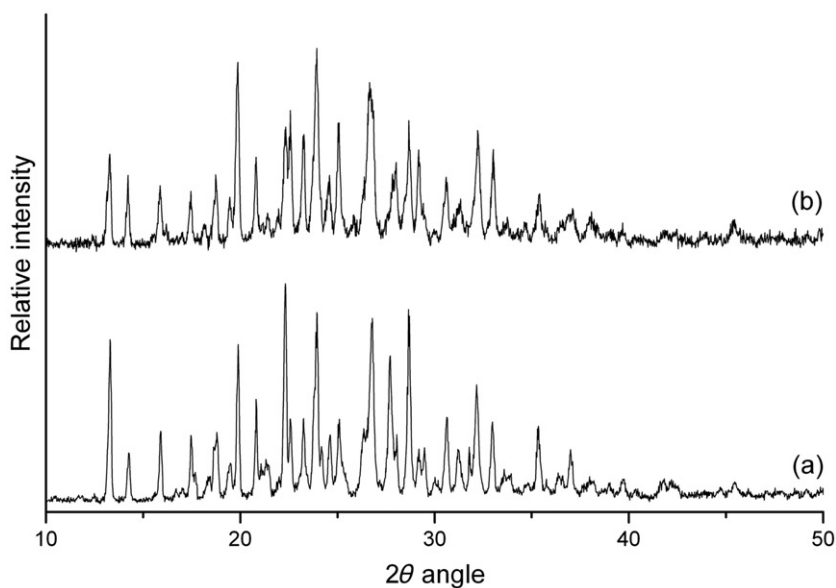


Figure 8. Powder X-ray diffraction patterns of **1**; initial sample (a) and after heating at 100°C for 4 h (b).

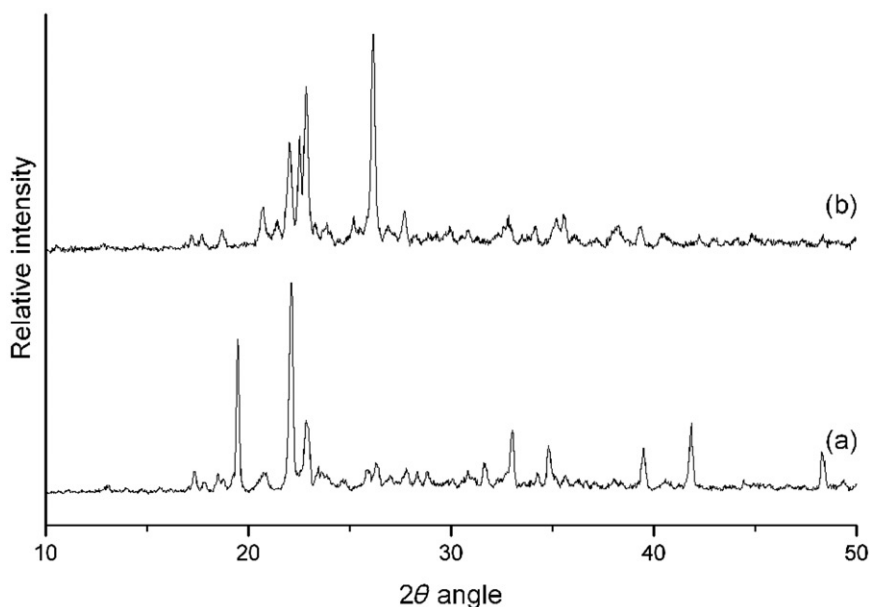


Figure 9. Powder X-ray diffraction patterns of **2**; initial sample (a) and after heating at 100°C for 4 h (b).

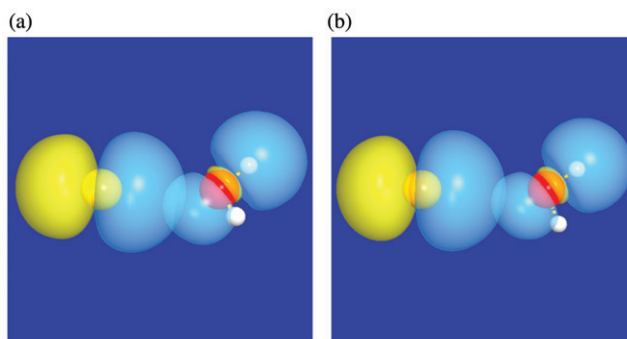
stabilizing the supramolecular architecture. In case of **2**, however, XRPD patterns show that the structure of **2** (figure 9a) is not retained upon heating at 100°C for 4 h (figure 9b) since $\text{NH}\cdots\text{Br}^-$ and $\text{OH}\cdots\text{Br}^-$ hydrogen-bonding interactions are weaker than the $\text{O}\cdots\text{Cl}^-$ and $\text{OH}\cdots\text{Cl}^-$ interactions observed in **1** (see also “X-ray crystal structure” Section 2.4).

2.7. The nature of the $\text{O}\cdots\text{X}$ interactions

Charge decomposition analysis (CDA) of the $\text{O}\cdots\text{Cl}^-$ and $\text{O}\cdots\text{Br}^-$ interactions at the CCSD(T)/6-311++G(d,p) level of theory reveal the charge transfer (CT) nature of the $\text{O}\cdots\text{Cl}^-$ and $\text{O}\cdots\text{Br}^-$ interactions with a net charge donation of 0.021 and 0.017 electrons from chloride and bromide to oxygen of coordinated water, respectively. The natural bond orbital (NBO) analysis predicted the specific $\text{lp}(\text{X}^-) \rightarrow \sigma^*(\text{O-H})$, donor–acceptor interactions. Stabilization energies $\Delta E(2)$ associated with $\text{lp}(\text{Cl}^-) \rightarrow \sigma^*(\text{O-H})$ and $\text{lp}(\text{Br}^-) \rightarrow \sigma^*(\text{O-H})$ CT interactions were 1.02 and 0.78 kcal mol^{-1} , respectively. The stabilization energy $\Delta E(2)$ associated with the CT interactions between the relevant donor–acceptor orbitals is computed from the second-order perturbative estimates of the Fock matrix in the NBO analysis according to the equation [17, 18]:

$$\Delta E(2) = \frac{q_i F_{ij}^2}{\varepsilon_i - \varepsilon_j}$$

This equation evaluates the magnitude of the donor–acceptor interaction in terms of the spatial overlap of the NBO, using the off-diagonal Fock-matrix elements F_{ij} and the



Scheme 6. 3-D isosurface plots of the $lp(Cl^-) \rightarrow \sigma^*(O-H)$ and $lp(Br^-) \rightarrow \sigma^*(O-H)$ interactions in the $Cl^- \cdots OH_2$ (a) and $Br^- \cdots OH_2$ (b) moieties of ionic salts **1** and **2**.

difference in energy between the NBOs, $\varepsilon_i - \varepsilon_j$, weighted by the occupancy of the donor NBO, q_i .

According to the NBO results the occupation of the antibonding $\sigma^*(O-H)$ MOs in the $Cl^- \cdots OH_2$ and $Br^- \cdots OH_2$ moieties was predicted to be 0.002 and 0.0015 $|e|$, respectively. The 3-D isosurface plots of the $lp(Cl^-) \rightarrow \sigma^*(O-H)$ and $lp(Br^-) \rightarrow \sigma^*(O-H)$ interactions are given in scheme 6.

3. Conclusion

In contrast to the ability of the thioamide 2-mercapto-benzimidazole (MBZIM) to form antimony(III) complexes with octahedral or square pyramidal geometries upon reaction with SbX_3 under aerobic conditions [4], 1,3-bis(3-pyridylmethyl)-2-thiourea (BPMTU) forms $3[HBPM TU]^+ \cdot 3[X]^- \cdot nH_2O$ ionic salts. All attempts to isolate Sb–BPMTU complexes with Sb–L coordination failed. Potentiometric determination of the pK_{α_1} for nitrogen-H ionization in BPMTU (1.73) indicated low nucleophilicity of sulfur which may be the cause for the non-formation of Sb–BPMTU complexes. For 2-mercapto-benzimidazole (L), however, the higher deprotonation constant of H_2L^+ to HL ($pK_{\alpha} = 2.69$) indicates higher nucleophilicity of the sulfur, thus accounting for the formation of stable complexes with Sb(III) of formula $SbCl_3L_2$ or $\{[SbCl_2L_4]^+ Cl^-\}$ [4]. The estimated nucleophilicity index ω^- for MBZIM and BPMTU of 0.096 and 0.072 eV at the B97D/6-311++G(d,p) level of theory illustrates the higher nucleophilicity of MBZIM than BPMTU. Mulliken net atomic charges on sulfur of MBZIM and BPMTU were -0.74 and -0.01 $|e|$ at the B97D/6-311++G(d,p) level; the sulfur of BPMTU is practically neutral, while that of MBZIM acquires a relatively high negative net atomic charge. Both the higher nucleophilicity and high negative net atomic charge on sulfur of MBZIM account for its high ligating ability to form a variety of complexes reported previously. In contrast, the lower nucleophilicity of BPMTU in conjunction with the neutrality of the sulfur explains why this ligand is not coordinated to $SbCl_3$, but affords water-soluble ionic salts.

The pK_{α_3} value for deprotonation of nitrogen of BPMTU is 5.35. The higher nitrogen proton affinity in BPMTU over MBZIM explains the easy formation of stable

HBPMTU⁺ when it hydrolyzes and therefore its inability to form complexes with SbX₃ as for MBZIM.

In ionic salt **1** quite strong supramolecular O⋯Cl⁻ interactions along with OH⋯Cl⁻ hydrogen bonding lead to the formation of 1-D zigzag tetrameric complexes consisting of four chlorides bridged by four waters through hydrogen bonds. Two oxygens of the bridging water are also coordinated to Cl⁻ forming a rhombus-shaped ring. CDA analysis of the O⋯Cl⁻ interactions at the CCSD(T) level of theory revealed the CT nature of the O⋯Cl⁻ interactions with a net charge donation of 0.021 electrons from chloride to oxygen. Accordingly in the weaker O⋯Br⁻ interactions occurring in **2** the net charge donation from bromide to coordinated water is 0.017 electrons at the same level of theory. The crystal structure of the chloride is interesting in that 1-D tetrameric chains are terminated by two NH⋯Cl⁻ hydrogen bonds from two HBPMTU⁺ ligands. Two chlorides are captured through hydrogen bonds in the free space between four tetrameric complexes of the crystal lattice forming the {[Cl(OH₂)⁻]₄}₄ 2Cl⁻ units. The Cl⋯Cl distance of 3.830 Å being slightly longer than the sum of van der Waals radii (3.62 Å) reflects the non-existence of closed-shell Cl⁻⋯Cl⁻ interactions. One Cl⁻ is anchored by four NH⋯Cl⁻ hydrogen bonds creating a noncovalent distorted tetrahedral coordination sphere around the Cl⁻, while the other Cl⁻ is anchored by two NH⋯Cl⁻ hydrogen bonds adopting a V-shaped coordination sphere (H⋯Cl⁻⋯H bond angle of 115.5°). The chloride anions hanging to NH hydrogens of HBPMTU⁺ in the crystal lattice of **1** is also supported by Raman and far-IR spectra. The ionic salt **1** does not lose water upon heating.

Hydrogen bonding and O⋯X interactions play an important role in the stability of the supramolecular architectures of **1** and **2**.

4. Experimental

4.1. Materials and instruments

All solvents used were of reagent grade; antimony(III) halides (Fluka) and 1,3-bis(3-pyridylmethyl)-2-thiourea (Aldrich, Merck) were used with no purification. C, H, N, and S elemental analyses were carried out with a Carlo Erba EA MODEL 1108 elemental analyzer. Melting points were measured in open tubes with a STUART scientific apparatus and are uncorrected. IR spectra from 4000 to 370 cm⁻¹ were obtained in KBr pellets while far IR spectra (400–50 cm⁻¹) were obtained in polyethylene discs with a Perkin–Elmer Spectrum GX FT-IR spectrometer. ¹H NMR spectra were recorded with a Bruker AC250 MHFT NMR instrument in D₂O with chemical shifts given in parts per million referenced to internal TMS(H). ESI-MS were acquired with a Micromass QToFTM quadrupole MS. All spectra of the complexes were recorded in time of flight (TOF) function, with a source temperature of 80°C, and low cone voltage (DCS = 100–120 V) to obtain gentle interface conditions. Micro FT-Raman measurements were carried out using near-IR laser radiation (Nd³⁺:YAG, 1064.1 nm). FT-Raman spectra (2.6 cm⁻¹ resolution) were recorded on a Bruker IFS-88 FT-IR/FRA-105 Raman module fitted with a Ge proprietary detector and coupled via two 1.0 m photooptic cables to a Nikon Optiphot-II optical microscope equipped with a Nikon 20x, super-long-range objective lens. Near-IR laser radiation was directed onto

the sample through the objective and collected along the same optical pathway in a 180° backscattering mode. Samples were measured as solid powders dispersed on a glass slide. Thermal studies were carried out on a Shimadzu DTG-60 simultaneous DTA-TG apparatus under N₂ flow (50 cm³ min⁻¹) with a heating rate of 10°C min⁻¹.

4.2. Synthesis and crystallization of {3[HBPMTU]⁺ · 3[X]⁻ · nH₂O}
 (BPM TU = 1,3-bis(3-pyridylmethyl)-2-thiourea, X = Cl⁻ and n = 1.5 (1),
 X = Br⁻ and n = 1 (2), X = I⁻ and n = 1 (3))

1.00 mmol 1,3-bis(3-pyridylmethyl)-2-thiourea (0.258 g) was dissolved in acetonitrile (10 cm³) and a solution of antimony(III) tri-halide (0.114 g SbCl₃, 0.179 g SbBr₃, 0.251 g SbI₃) in methanol (10 cm³) was then added to the above solution. This solution was stirred for 1 h and the resulting precipitate was filtered off and dried at room temperature. Complex **1** is soluble in water, methanol, ethanol, DMSO, and DMF.

(1): White crystal, yield 74%, m.p.: 116–118°C, mw: 920.44 g mol⁻¹. Elemental analysis, Found: C, 51.25; H, 5.12; N, 17.95; S, 10.24. Anal. Calcd for C₃₉H₄₈Cl₃N₁₂O_{1.5}S₃: C, 51.40; H, 5.30; N, 18.44; S, 10.55. IR(cm⁻¹): 3237s, 3048m, 1556s, 1477m, 1416m, 1374w, 1346w, 1296m, 1185w, 1050m, 970w, 938w, 801m, 687s, 543m. ¹H-NMR (ppm) in D₂O: 8.56–8.54 ppm (aromatic protons b and c), 8.17–8.14 and 7.77–7.71 ppm (protons e and d, respectively), 4.81 ppm (aliphatic protons f). MS *m/z*: 293.4 [LH⁺.Cl⁻]⁻.

(2): White crystal, yield 76%, m.p.: 116–119°C, mw: 1053.79 g mol⁻¹. Elemental analysis, Found: C, 45.64; H, 4.27; N, 16.14; S, 9.04. Anal. Calcd for C₃₉H₄₇Br₃N₁₂O₁S₃: C, 45.23; H, 4.57; N, 16.23; S, 9.29. IR(cm⁻¹): 3234s, 3052s, 1538s, 1457w, 1417m, 1347m, 1294m, 1051m, 969m, 936m, 802m, 688s, 544m. ¹H-NMR (ppm) in D₂O: 8.59–8.57 ppm (aromatic protons b and c), 8.27–8.24 and 7.84–7.79 ppm (protons e and d, respectively), 4.84 ppm (aliphatic protons f). MS *m/z*: 338.7 [LH⁺.Br⁻]⁻.

(3): Yellow crystal, yield 72%, m.p.: 137–139°C, mw 1194.79 g mol⁻¹. Elemental analysis, Found: C, 39.56; H, 4.01; N, 13.92; S, 7.93. Anal. Calcd for C₃₉H₄₉I₃N₁₂O₂S₃: C, 39.81; H, 4.02; N, 14.28; S, 8.17. IR(cm⁻¹): 3230s, 3060s, 2909w, 1617w, 1545s, 1483w, 1430m, 1378w, 1324m, 1288m, 1188m, 1052m, 964m, 929m, 828w, 788m, 689s, 547m. ¹H-NMR (ppm) in D₂O: 8.56–8.54 ppm (aromatic protons b and c), 8.19–8.16 and 7.77–7.72 ppm (protons e and d, respectively), 4.82 ppm (aliphatic protons f). MS *m/z*: 385.2 [LH⁺.I⁻]⁻.

4.3. X-ray structure determination

Data for **1** were collected on a Nonius Kappa CCD area detector (ϕ scans and ω scans) in the range 3.06–27.48°, using graphite-monochromated Mo-K α ($\lambda = 0.71073 \text{ \AA}$) at 120(2) K, controlled by the Collect software package [19a]. The data were processed by Denzo [19b] and corrected for absorption using SADABS [19c]. The structures were solved by direct methods and refined by full-matrix least-squares on all F_o^2 data using SHELXS-97 [19d] and SHELXL-97 [19e]. All non-hydrogen atoms were refined

anisotropically with hydrogens included in idealized positions and refined using a riding model.

Intensity data for crystals of **2** were collected on an Oxford Diffraction CCD instrument [20a] using graphite-monochromated Mo radiation ($\lambda = 0.71073 \text{ \AA}$). All data were corrected for Lorentz-polarization effects and absorption [20a,b]. The structures were solved with direct methods using *SHELXS97* [19d] and refined by full-matrix least-squares on F^2 with *SHELXL97* [19e]. All non-hydrogen atoms were refined anisotropically; hydrogens were located at calculated positions and refined *via* the “riding model” with isotropic thermal parameters fixed at 1.2 (1.3 for CH_3 groups) times the U_{eq} value of the appropriate carrier atom.

1: $\text{C}_{39}\text{H}_{48}\text{Cl}_3\text{N}_{12}\text{O}_{1.50}\text{S}_3$, monoclinic in $P2_1/n$, $a = 12.9746(3) \text{ \AA}$, $b = 22.2176(5) \text{ \AA}$, $c = 15.5500(4) \text{ \AA}$, $\beta = 107.9010(10)^\circ$, $V = 4265.51(18) \text{ \AA}^3$, $Z = 4$, $T = 120(2) \text{ K}$, $\rho(\text{Calcd}) = 1.419 \text{ g cm}^{-3}$, $\mu = 0.412 \text{ mm}^{-1}$, reflections collected: total, uniq. data, $R(\text{int})$ 57428, 9753, 0.0992, respectively, index range: $-16 < h < 16$, $-28 < k < 28$, $-19 < l < 20$, final R^a , $wR2^b$ [$I > 2\sigma(I)$] indices: 0.0512 and 0.1120, respectively. ($^a R = \sum ||F_o| - |F_c|| / \sum |F_o|$; $^b wR2 = [\sum w(F_o^2 - F_c^2)^2 / \sum w(F_o^2)^2]^{1/2}$); goodness of fit: 1.031.

2: $\text{C}_{39}\text{H}_{47}\text{Br}_3\text{N}_{12}\text{O}_1\text{S}_3$, monoclinic in $P2_1/n$, $a = 13.0049(2)$, $b = 22.5144(3)$, $c = 15.7138(3) \text{ \AA}$, $\beta = 109.062(2)^\circ$, $V = 4348.67(13) \text{ \AA}^3$, $Z = 4$, $T = 100(2) \text{ K}$, $\rho(\text{Calcd}) = 1.579 \text{ g cm}^{-3}$, $\mu = 2.975 \text{ mm}^{-1}$, reflections collected: total, uniq. data, $R(\text{int})$ 28587, 7643, 0.042, respectively, index range: $-15 < h < 13$, $-26 < k < 26$, $-15 < l < 18$, final R^a , $wR2^b$ [$I > 2\sigma(I)$] indices: 0.0311, 0.0651. ($^a R = \sum ||F_o| - |F_c|| / \sum |F_o|$; $^b wR2 = [\sum w(F_o^2 - F_c^2)^2 / \sum w(F_o^2)^2]^{1/2}$); goodness of fit: 0.92.

4.4. X-ray powder diffraction

X-ray powder diffraction patterns were obtained using a Bruker AXS D8-Advance Diffractometer in Bragg-Brentano geometry equipped with a Cu sealed-tube radiation source ($\lambda = 1.54178 \text{ \AA}$) and a secondary beam graphite monochromator. The 2θ range used in the measurements was from 10 to 50° in steps of 0.02° with a count time of 5 s per step.

4.5. Potentiometric titration

Potentiometric titrations of *N,N*-bis(3-pyridylmethyl)thiourea were carried out at 298 K under argon using a total volume of 2.5 mL . The titrations were performed at a constant ionic strength of 0.1 mol dm^{-3} (KNO_3) over the pH range 2 – 11 on a MOLSPIN pH-meter system (Molspin automatic titrator, Molspin Ltd., Newcastle upon-Tyne, UK), using a 0.500 mL micrometer syringe and a combined glass-silver chloride electrode calibrated in hydrogen concentrations using HNO_3 [21a]. KOH (0.1 mol L^{-1}) was used as titrant. The concentration of the ligand used was 2 mol L^{-1} . The experimental data were analyzed using the HYPERQUAD program [21b]. Standard deviations computed by HYPERQUAD refer to random errors.

4.6. Computational details

All calculations were carried out using the GAUSSIAN09 software package [22] and the results were obtained by employing density functional theories (DFT). The geometries were fully optimized using the full-range PBE0 non local hybrid GGA functional [7–10] and the dispersion corrected GGA B97-D functional developed by Grimme [11] combined with the 6-311++G(d,p) basis set. CDA was performed at the CCSD(T)/6-311++G(D,p) level as implemented in the *AOMix* program [23]. NBO calculations were carried out using the NBO 5.0 program [18] run through Gaussian09 [22]. The stationary points found on the PESs as a result of the geometry optimizations of MBZIM and BPMTU have been tested to represent energy minima rather than saddle points *via* harmonic vibrational analysis.

Supplementary material

Crystallographic data (excluding structure factors) for the structures reported in this article have been deposited at the Cambridge Crystallographic Data Centre as supplementary publication CCDC no. 649658 (1) and 748166 (2). Copies of the data can be obtained free of charge on application to CCDC, 12 Union Road, Cambridge CB2 1EZ, UK (Fax: (+44) 1223-336-033; E-mail: deposit@ccdc.cam.ac.uk).

Acknowledgments

This research was carried out in partial fulfillment of the requirements for the Ph.D. thesis of Ozturk under the supervision of Hadjikakou. The Hellenic Ministry of Education is also acknowledged for the Gr–Tr scholarship to Ozturk, Hadjikakou, Hadjiliadis, and Butler would like to acknowledge a NATO grant for the exchange of scientists.

References

- [1] (a) R. Custelcean, M.G. Gorbunova. *J. Am. Chem. Soc.*, **127**, 16362 (2005); (b) C.A. Bremner, M. Simpson, W.T.A. Harrison. *J. Am. Chem. Soc.*, **124**, 10960 (2002); (c) R. Custelcean, D. Jiang, B.P. Hay, W. Luo, B. Gu. *Cryst. Growth Des.*, **8**, 1909 (2008).
- [2] (a) J.E.F. Reynolds, A.B. Prasad (Eds), *Martindale: The Extra Pharmacopoeia*, 28th Edn.: The Pharmaceutical Press, London, UK (1982); (b) E. De Clercq. *Clin. Microbiol. Rev.*, **10**, 674 (1997); (c) E. De Clercq. *Int. J. Antimicrob. Agents*, **18**, 309 (2001).
- [3] (a) M.N. Xanthopoulou, S.K. Hadjikakou, N. Hadjiliadis, E.R. Milaeva, J.A. Gracheva, V.-Y. Tyurin, N. Kourkoumelis, K.C. Christoforidis, A.K. Metsios, S. Karkabounas, K. Charalabopoulos. *Eur. J. Med. Chem.*, **43**, 327 (2008); (b) M.N. Xanthopoulou, S.K. Hadjikakou, N. Hadjiliadis, N. Kourkoumelis, E.R. Milaeva, Y.-A. Gracheva, V.Y. Tyurin, I. Verginadis, S. Karkabounas, M. Baril, I.S. Batler. *Russ. Chem. Bull.*, **56**, 767 (2007); (c) M.N. Xanthopoulou, S.K. Hadjikakou, N. Hadjiliadis, M. Kubicki, S. Skoulika, T. Bakas. *Inorg. Chem.*, **46**, 1187 (2007); (d) V.I. Balas, S.K. Hadjikakou, N. Hadjiliadis, N. Kourkoumelis, M.E. Light, M. Hursthouse, A.K. Metsios, S. Karkabounas, *Bioinorganic Chemistry and Applications*, Article ID 654137, doi:10.1155/2008/654137, (2008); (e) M.N. Xanthopoulou, S.K. Hadjikakou, N. Hadjiliadis, M. Schurmann, K. Jurkschat, A. Michaelides, S. Skoulika, T. Bakas, J.J. Binolis, S. Karkabounas, K. Charalabopoulos. *J. Inorg. Biochem.*, **96**, 425 (2003).

- [4] (a) I.I. Ozturk, S.K. Hadjidakou, N. Hadjiliadis, N. Kourkoumelis, M. Kubicki, M. Baril, I.S. Butler, J. Balzarini. *Inorg. Chem.*, **46**, 8652 (2007); (b) I.I. Ozturk, S.K. Hadjidakou, N. Hadjiliadis, N. Kourkoumelis, M. Kubicki, A.J. Tasiopoulos, H. Scleiman, M.M. Barsan, I.S. Butler, J. Balzarini. *Inorg. Chem.*, **48**, 2233 (2009); (c) I. Ozturk, S. Filimonova, S.K. Hadjidakou, N. Kourkoumelis, V. Dokorou, M.J. Manos, A.J. Tasiopoulos, M.M. Barsan, I.S. Butler, E.R. Milaeva, J. Balzarini, N. Hadjiliadis. *Inorg. Chem.*, **49**, 488 (2010).
- [5] (a) S.K. Hadjidakou, C.D. Antoniadis, N. Hadjiliadis, M. Kubicki, J. Binolis, S. Karkabounas, K. Charalabopoulos. *Inorg. Chim. Acta*, **358**, 2861 (2005); (b) L. Ghys, M. Biesemans, M. Gielen, A. Garoufis, N. Hadjiliadis, R. Willem, J.C. Martins. *Eur. J. Inorg. Chem.*, 513 (2000); (c) Z. Yang, T. Bakas, A. Sanchez-Diaz, K. Charalabopoulos, J. Tsangaris, N. Hadjiliadis. *J. Inorg. Biochem.*, **72**, 133 (1998).
- [6] (a) K. Kahmann, H. Sigel, H. Erlenmeyer. *Helv. Chim. Acta*, **47**, 1754 (1964); (b) J. Catalan, J.L.M. Abbound, J. Elguero. *Adv. Heterocycl. Chem.*, **41**, 248 (1986); (c) D.C. Ghosh, J. Jana. *Int. J. Quantum Chem.*, **92**, 484 (2003).
- [7] (a) C. Adamo, V. Barone. *Chem. Phys. Lett.*, **274**, 242 (1997); (b) C. Adamo, V. Barone. *J. Chem. Phys.*, **110**, 6160 (1999); (c) C. Adamo, G.E. Scuseria, V.J. Barone. *Chem. Phys.*, **111**, 2889 (1999); (d) C. Adamo, V. Barone. *Theor. Chem. Acc.*, **105**, 169 (2000); (e) V. Vetter, C. Adamo, P. Maldivi. *Chem. Phys. Lett.*, **325**, 99 (2000).
- [8] M. Ernzerhof, G.E. Scuseria. *J. Chem. Phys.*, **110**, 5029 (1999).
- [9] M. Bühl, C. Reimann, D.A. Pantazis, T. Bredow, F. Neese. *J. Chem. Theory Comput.*, **4**, 1449 (2008).
- [10] C.J. Cramer, D.G. Truhlar. *Phys. Chem. Chem. Phys.*, **11**, 10757 (2009) and references therein.
- [11] S. Grimme. *J. Comput. Chem.*, **27**, 1787 (2006).
- [12] C.S. Lai, E.R.T. Tiekink. *Acta Crystallogr., Sect. E: Struct. Rep. Online*, **58**, o538 (2002).
- [13] (a) P. Jaramillo, P. Pérez, R. Contreras, W. Tiznado, P. Fuentealba. *J. Phys. Chem. A*, **110**, 8181 (2006); (b) P. Jaramillo, P. Fuentealba, P. Pérez. *Chem. Phys. Lett.*, **427**, 421 (2006).
- [14] (a) A. Bondi. *J. Phys. Chem.*, **68**, 441 (1964); (b) R.D. Shanon. *Acta Crystallogr., Sect. A*, **32**, 751 (1976).
- [15] J.P.M. Lommerse, A.J. Stone, R. Taylor, F.H. Allen. *J. Am. Chem. Soc.*, **118**, 3108 (1996).
- [16] (a) J.E. Cahill, G.E. Leroi. *J. Chem. Phys.*, **51**, 4514 (1969); (b) S.H. Walmsley, A. Anderson. *Mol. Phys.*, **7**, 411 (1964).
- [17] (a) F. Weinhold. In *The Encyclopedia of Computational Chemistry*, P.v.R. Schleyer (Ed.), pp. 1792–1811, Wiley, Chichester, U.K. (1998); (b) A.E. Reed, L.A. Curtiss, F. Weinhold. *Chem. Rev.*, **88**, 899 (1988); (c) V. Pophristic, L. Goodman. *Nature*, **411**, 565 (2001); (d) F. Weinhold. *Nature*, **411**, 539 (2001); (e) A.B. Chaplin, J.A. Harrison, P.J. Dyson. *Inorg. Chem.*, **411**, 565 (2005); (f) F. Weinhold, C.R. Landis, *Valency and Bonding: A Natural Bond and Orbital Donor-Acceptor Perspective*, Cambridge University Press, New York (2005).
- [18] E.D. Glendering, J.K. Badenhop, A.E. Reed, J.E. Carpenter, J.A. Bohmann, C.M. Morales, F. Weinhold, *NBO (version 5.0)*, Theoretical Chemistry Institute, University of Wisconsin, Madison, WI (2001).
- [19] (a) R. Hoft, Collect, Data Collection Software, Nonius, The Netherlands (1998); (b) Z. Otwinowski, W. Minor. In *Methods in Enzymology: Macromolecular Crystallography*, C.W. Carter Jr and R.M. Sweet (Eds.), Part A, vol. 276, pp. 307–326, Academic Press, New York (1997); (c) G.M. Sheldrick. *SADABS – Bruker Nonius Area Detector Scaling and Absorption Correction–V2.10*, University of Göttingen, Germany (2003); (d) G.M. Sheldrick. *Acta Cryst.*, **A46**, 467 (1990); (e) G.M. Sheldrick, *SHELXS-97, Program for Crystal Structure Solution*, University of Göttingen, Germany (1997).
- [20] (a) Oxford Diffraction. *CRYSTALIS CCD and CRYSTALIS RED (Version p171.29.2)*, Oxford Diffraction Ltd., Abingdon, Oxford, England (2006); (b) Oxford Diffraction. *CrysAlis RED (Version 1.171.31.5), (release 28-08-2006 CrysAlis171.NET)*, Oxford Diffraction Ltd., Abingdon, Oxford, England (2006).
- [21] (a) H. Irving, M.G. Miles, L.D. Pettit. *Anal. Chim. Acta*, **38**, 475 (1967); (b) A. Sabatini, A. Vacca. *Talanta*, **43**, 1739 (1996).
- [22] M.J. Frisch, G.W. Trucks, H.B. Schlegel, G.E. Scuseria, M.A. Robb, J.R. Cheeseman, G. Scalmani, V. Barone, B. Mennucci, G.A. Petersson, H. Nakatsuji, M. Caricato, X. Li, H.P. Hratchian, A.F. Izmaylov, J. Bloino, G. Zheng, J.L. Sonnenberg, M. Hada, M. Ehara, K. Toyota, R. Fukuda, J. Hasegawa, M. Ishida, T. Nakajima, Y. Honda, O. Kitao, H. Nakai, T. Vreven, J.A. Montgomery Jr, J.E. Peralta, F. Ogliaro, M. Bearpark, J.J. Heyd, E. Brothers, K.N. Kudin, V.N. Staroverov, R. Kobayashi, J. Normand, K. Raghavachari, A. Rendell, J.C. Burant, S.S. Iyengar, J. Tomasi, M. Cossi, N. Rega, J.M. Millam, M. Klene, J.E. Knox, J.B. Cross, V. Bakken, C. Adamo, J. Jaramillo, R. Gomperts, R.E. Stratmann, O. Yazyev, A.J. Austin, R. Cammi, C. Pomelli, J.W. Ochterski, R.L. Martin, K. Morokuma, V.G. Zakrzewski, G.A. Voth, P. Salvador, J.J. Dannenberg, S. Dapprich, A.D. Daniels, O. Farkas, J.B. Foresman, J.V. Ortiz, J. Cioslowski, D.J. Fox, *Gaussian 09, Revision A.02*, Gaussian, Inc., Wallingford, CT (2009).
- [23] S.I. Gorelsky, S. Ghosh, E.I. Solomon. *J. Am. Chem. Soc.*, **128**, 278 (2006); (b) S.I. Gorelsky, A.B.P. Lever. *J. Organomet. Chem.*, **635**, 187 (2001); (c) S.I. Gorelsky. *AOMix*, Department of Chemistry, York University, Toronto, ON (1997). Available online at: <http://www.sg-chem.net> (accessed 11 December 2010).